Fabrication and photocatalysis of BiFeO$_3$ with inverse opal structure

Tianya Tan[1] · Wang Xie[1] · Guangju Zhu[1] · Jing Shan[1] · Panfeng Xu[1] ·
Lina Li[1] · Jiwei Wang[1]

Abstract The bismuth ferrite (BiFeO$_3$, BFO) with a face-centered cubic inverse opal structure was prepared by the sol–gel method, involving the infiltration of liquid precursors into polystyrene (PS) colloidal crystals and the post-annealing for the remove of PS and the crystallization of BFO. This inverse opals exhibit a continuous 3D photonic crystal structure consisting of single phase BFO. The photocatalytic investigation reveals that the degradation rate of Rhodamine B under UV–vis light irradiation is 1.4 times that of the conventional BFO film without the high periodic porous structure. The high surface area, slow photon and light scattering effects due to the photonic crystal structure are responsible for the enhanced photocatalysis of BFO inverse opal. This work is expected to improve the comprehensive performance of BFO by integrating the photonic effect together with its ferromagnetic and visible-light-driving catalysis properties.

Keywords Inverse opal structure · Photocatalysis · Porous materials · Photonic crystal · Sol–gel preparation

1 Introduction

Among metal-oxide photocatalysts, TiO$_2$ is one of the most famous photocatalysts because of the relatively high reactivity, low cost, chemical stability and non-toxicity [1–3]. However, TiO$_2$ can only become active under ultraviolet irradiation due to the wide bandgap ($\sim$3.2 eV) and only a small fraction of solar light (3–5 %) can be utilized [4]. Recently, the photocatalytic activity of bismuth ferrite (BFO) has attracted more attention for the visible-light-driven photocatalysis due to the small bandgap ($\sim$2.18 eV) [5–7] and the multiferroic properties. Therefore, considerable efforts have been devoted to develop the comprehensive performances of BFO by modifying its feature and structure.

Increasing surface reaction sites through fabricating hierarchical nanostructures is a common and effective way to improve the photocatalytic efficiency. Consequently, nanoparticle, thin film and mesoporous structures are developed to achieve the larger specific surface area [8–10]. Comparing to disorder porous structures, an inverse opal BFO with ordered macroporous structure can not only provide more surface area but also exhibit many desirable optical properties of the photonic crystal, such as photonic bandgap (PBG), light scattering and slow photon effects [11, 12]. The slow photon effect due to the group velocity of photons near photonic bandgap (PBG) slowing down, can result in the remarkable increase of the light path length. Thereby the absorption of the photocatalyst is greatly enhanced when the wavelength of slow photon overlaps the electronic bandgap [1, 13, 14]. It should be pointed that the competition between the slow photon enhancement and the PBG reflectivity must be considered under white-light irradiation [15]. Fortunately, by modulating the position of PBG based on the large absorption region of the photocatalyst, the PBG reflectivity can be avoided and the slow photon enhancement can be allowed to dominate. The position of PBG will shift to the shorter wavelength when the incident angle increases according to Bragg's law. Therefore, the dependence of the incident angle on the slow photon effect should also be considered in experiments.

✉ Jiwei Wang
  jiweiwang6688@yahoo.com

[1] College of Physics, Liaoning University, No.66 Chongshan middle Road, Shenyang 110036, China

A certain quantity of TiO$_2$-based photonic crystal photocatalysts amplifying photochemistry efficiency are reported in recent years [1, 12–14]. However, very few reports of BiFeO$_3$-based photonic crystal photocatalysts are available. Introducing "photonic effect" into this multiferroic material not only improves its phtocatalysis efficiency but also develops its multifunctional performances. As a move in these directions, we fabricate the BFO with the inverse opal structure and investigate its photocatalytic properties comparing with conventional BFO films. This work is expected to open up new perspectives on the development of highly efficient multifunctional photocatalysts.

2 Experimental

The monodisperse polystyrene (PS) microspheres were synthesized by the emulsifier-free emulsion polymerization of styrene using potassium persulfate as the initiator. The synthesized spheres with the diameter of 440 nm were self-assembled on fluorine-doped tin oxide (FTO) glass substrates to fabricate the opal structures by the float controlled vertical deposition (FCVD) technique.

Liquid precursors were prepared by dissolving a certain amount of citric acid in a mixture solution of distilled water and ethanol (1:1), and then adding a stoichiometric metal nitrates. In this experiment, the solution concentration was 0.27 mol/L, while its pH value was acidized to 1 by adding nitric acid. The self-assembled opal structures on the glass substrates were dipped in this precursor solution, and thus the voids among these colloidal spheres were filled by the sol solution through the capillary action. Then the samples were putted into a vacuum oven at 50 °C for 30 min to form a precursor gel in the voids. The infiltration for colloidal crystals with BFO precursors was repeated 2–3 times to make sure that all the voids among the colloidal spheres were completely filled. Finally, the samples were heated from room temperature to 500 °C with 0.5 °C/min rate, followed by annealing for 1 h in air to remove polystyrene opals. A highly ordered replica consisting of BFO framework with air holes was obtained. Meanwhile, the BFO films were prepared for 16 layers on the FTO glass substrates with the precursor solution by the spin-coating method to reach the same thickness as that of inverse opal structures, and followed by the same annealing process. The phase identification and the purity of the samples were analyzed by an X-ray diffractometer (Brucker D8 Advanced). SEM images were taken by a LEO1530 scanning electron microscopy.

A 100 ml cubic quartz glass with 40 ml reaction solution was used as the photocatalytic reactor. Both BFO inverse opal structure and BFO film were selected 0.25 cm^2

and immersed in 10 mg/L Rhodamine B (RhB) solution. At every 10 min interval, 1 ml solution irradiated by the UV–vis light was taken out and measured by a Lambda 950 UV–visible spectrophotometer. According to the decolourization absorbance, the photocatalytic degradation ratio of the dye solution was calculated.

3 Results and discussion

Figure 1 shows the XRD patterns of the inverse BFO opals using 440 nm PS spheres as a template by annealing precursor gels. According to the JCPDS card (No: 86-1518), the prepared BFO opals presented the single phase with the lattice constants of $a = b = 0.5577$ nm and $c = 1.3862$ nm. Figure 2a and b show the SEM images of the PS opal structure template and the inverse opal BFO network structure with air spheres, respectively. The face-centered-cubic (fcc) structure of the PS with the (111) closed-packed surface exhibits the opal structure, while an interconnected network structure with air spheres inheriting the fcc order of the PS opal template demonstrates that the inverse opal structure maintained very well after the annealing process. It is observed that the BFO inverse opals contained highly ordered hexagonal air spheres with a diameter of around 270 nm, indicating the shrinkage of about 38 % compared to the original opal template. This shrinkage results in a substantial isotropic compressive stress in samples that may cause the break-up and appearance of defects. Even though some disorders appear, the sample is still arranged in order for long scale as shown in Fig. 2b. Figure 3 shows the absorption spectra of the BFO with and without the inverse opal structure, respectively. The cut-off adsorption wavelength (shown in inner figure) of the BFO thin film without the inverse opal structure is around 570 nm (~2.18 eV), which indicates that the visible light is efficient for its photocatalysis. The absorption of the BFO inverse opal presents the same
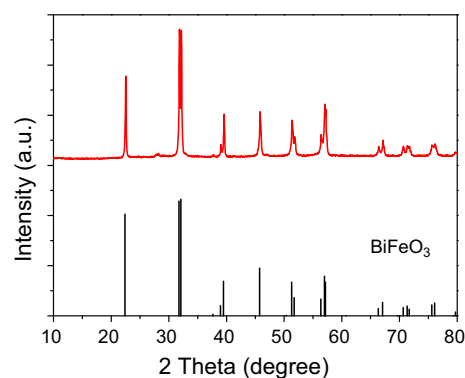
Fig. 1 XRD patterns of the inverse BFO opals using 440 nm polystyrene spheres as a template by annealing precursor gel
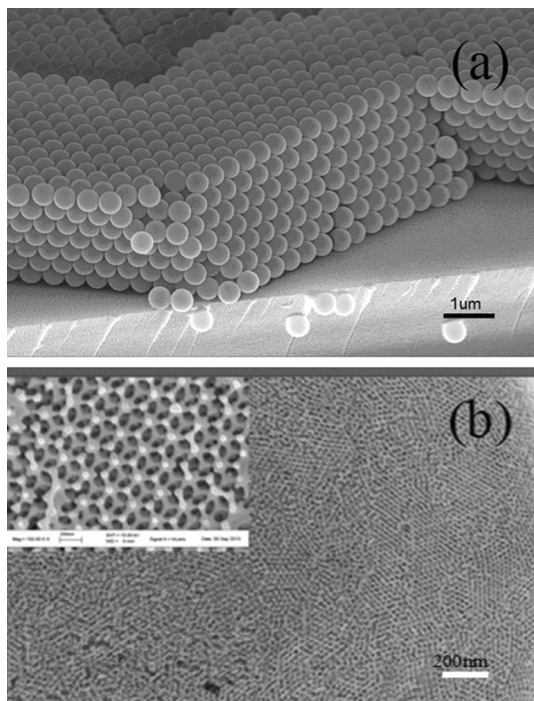
Fig. 2 SEM images: **a** PS opal structures; **b** BFO inverse opal structures
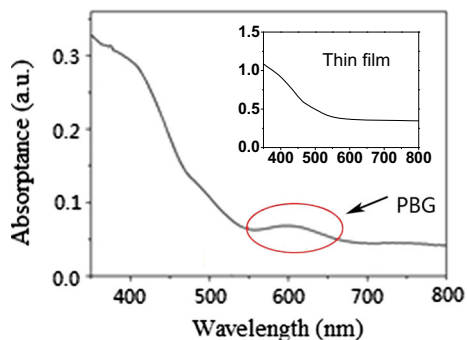
Fig. 3 The UV–visible absorption spectra of the BFO with and without inverse opal structures (inner figure)

electronic bandgap (~ 2.18 eV) as that of the conventional BFO thin film. Besides, there exists an enhanced absorption band from 550 to 650 nm resulting from the high periodic porous structures, i.e., the PBG of BFO, which can also be confirmed by calculating the location of PBG considering the factors of pore size, refractivity of BFO and volume filling fraction [1]. At the wavelength edges of the PBG, photons propagate with the strongly reduced group velocity, therefore the absorption tends to be reinforced owing to the increase of the effective optical path length. It is noted that the blue edge of PBG partly overlaps the electronic bandgap of BFO as shown in Fig. 3. In this condition, the PBG reflectivity can not preclude the absorption
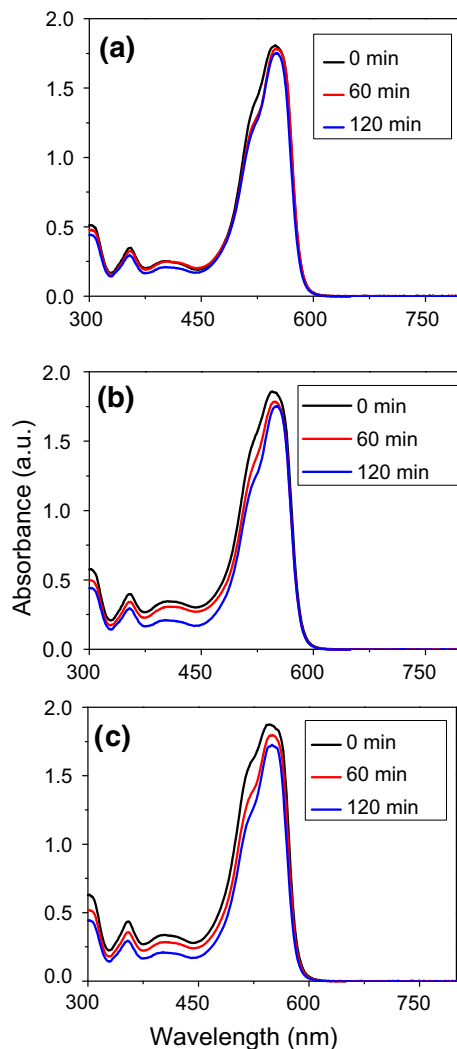
Fig. 4 The absorption spectra of RhB decolorization for various structures: **a** FTO glass; **b** BFO film; **c** BFO inverse opals

of BFO [15], meanwhile the slow photon effect should contribute to the photocatalysis enhancement of BFO inverse opal.

Figure 4a–c show the absorption spectra of the RhB photocatalytic degradation for FTO glass substrates, BFO films, BFO inverse opals, respectively. The direct degradation of RhB on the FTO glass substrate served as a base line. Meanwhile, the degradation on BFO films was conducted for the comparison to that for BFO inverse opal structure. The decolourization ratio of RhB can be calculated by the formula $D = (A_0 - A_t)/A_0 \times 100\%$, where A_0 is the absorbance index of the maximum absorption wavelength at the beginning, and A_t is that at time t. The presence of the BFO film improved the photodegradation of RhB under the UV–vis light irradiation with the decolourization ratio of 5.6 % for 2 h, shown in Fig. 4b. While the decolourization ratio for BFO inverse opals
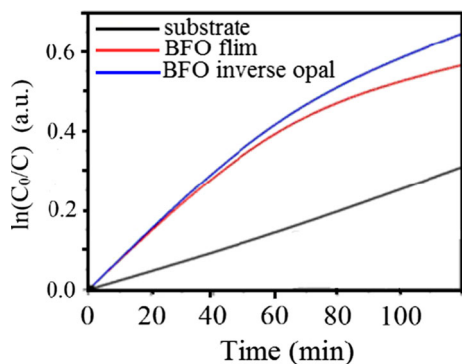
Fig. 5 The kinetics of the photocatalytic degradation of RhB on the different BFO films under UV–vis light irradiation

structure was even better than that for the BFO film. 7.84 % RhB was degraded in the same experimental conditions as shown in Fig. 4c. These results reveal that the apparent reaction rate constant of RhB degradation for the BFO inverse opal structure is 1.4 times that for the conventional BFO film without an ordered porous structure. The kinetics of the photocatalytic degradation of RhB was able to be depicted by the pseudo-first-order kinetics equation: $\ln(C_0/C) = K_t$, where K_t is the kinetic constant, C_0 is the initial concentration of RhB and C is that at time t. The kinetic constants were calculated from the slope of the linear correlation, the kinetic constant of BFO inverse opals was 1.15 times as that of BFO films as shown in Fig. 5.

The superiority of the BFO inverse opal structure over the BFO film is attributed to the more reaction area offered by the open macroporous structure. In addition, the inverse opal structure is a kind of 3D photonic crystal, the above-mentioned light scattering and the slow photon effect should also contribute to the photocatalytic enhancement when the PBG is in position. As shown in Fig. 3, the PBG overlaps the absorption tail of BFO, so the effect of PBG reflectivity on absorption is negligible. While the slow photon effect at the PBG edge and multiple scatterings among the photonic crystal segments reinforce the interaction between the light and the matter [7, 12]. In experiments, the incident angle of the light deviates from the normal angle due to the sizes of xenon lamp and samples in deed, thus the blue PBG edge should be blue shifting and overlapped more absorption band of BFO, resulting in the strong slow photon enhancement for photocatalysis [14].

Considering these advantages, 40 % additional photocatalysis seems not to represent the total efficiency of the BFO inverse opal structure. It is noticed that the same thickness of the BFO film was selected to compare the photocatalytic efficiency with the BFO inverse opal, thus the mass of the BFO film without macroporous structures must be much more than that of BFO inverse opals. Actually, the number of layers participating in photocatalysis

depends on the migration distance of photo-generated carriers, which is usually several hundred nanometers for semiconductors. In this case, not only the surface but also sublayers of BFO film may contribute to photocatalysis. But for the BFO inverse opal structure, the flowability and cyclicity of the dye solution in macroporous structures cannot be as good as that on the film surface, meanwhile the interface impurity and the structure collapse may be formed during the process of removing PS opals. All these may decrease the actual photocatalytic efficiency of BFO inverse opals and thus preclude its advantages over the conventional BFO film. These factors for BFO inverse opals are able to be overcome through optimizing the preparation techniques and photocatalytic reaction conditions. Thereby the light scattering effect and the phenomenon of the slow photon in the inverse opal structure should provide BFO inverse opals with particular advantages besides the big specific surface area. Our experiments have demonstrated that the ordered macroporous inverse opal structures can enhance the photocatalytic activity of BFO, and forming multifunctional materials is possible. It is also a good example of introducing photonic crystal structure to many processes relating to light absorption such as solar cells and optical communications.

4 Conclusions

The BFO with high periodic fcc inverse opal structures were fabricated by sol–gel method. The PBG overlapping the electronic bandgap tail is confirmed by comparison of BFO with and without the inverse opal structure, so the slow photon at the PBG edge and multiple scatterings reinforce the interaction between the light and the matter. Therefore the enhanced phtocatalysis is not only origin of the high surface area, but also the slow photon and light scattering effects. Meanwhile the low flowability and cyclicity of the solution, extra interface impurity and structure collapse may weaken the photocatalytic activities. This work is an important preliminary step of summing up advantages of the order porous and ferromagnetic properties, in particular of constructing the photonic crystal structure to improve the photocatalytic efficiency and realize the goal of integration multifunctional photocatalyst.

References

1. J. Liu, G.L. Liu, M.Z. Li, W.Z. Shen, Z.Y. Liu, J.X. Wang, Energy Environ. Sci. **39**, 1503 (2010)

2. S.N. Frank, A. Bard, J. Am. Chem. Soc. **99**, 303 (1977)
3. S.W. Lee, J. Drwiega, D. Mazyck, C.Y. Wu, W.M. Sigmund, Mater. Chem. Phys. **96**, 483 (2006)
4. O. Teruhisa, T. Toshiki, T. Maki, L. Ryoji, Catal. Lett. **98**, 255 (2004)
5. F. Gao, S. Dong, F. Yuan, T. Yu, J.M. Liu, Adv. Mater. **19**, 2889 (2007)
6. K. Takahashi, N. Kida, M. Tonouchi, Phys. Rev. Lett. **96**, 117402 (2006)
7. J. He, R.Q. Guo, L. Fang et al., Mater. Res. Bull. **48**, 3017 (2013)
8. F. Sordello, C. Minero, Appl. Catal. B-Environ. **163**, 452 (2015)
9. W.F. Liu, A.J. Wang, J.J. Tang et al., Micropor. Mesopor. Mat. **204**, 143 (2015)
10. Z.Y. Hu, L.B. Xu, L.L. Wang, Y. Huang et al., Catal. Commun. **40**, 106 (2013)
11. M. Wu, J. Liu, J. Jin, C. Wang et al., Appl. Catal. B Environ. **150–151**, 411 (2014)
12. H. Chen, S. Chen, X. Quan, Y. Zang, Environ. Sci. Technol. **44**, 451 (2010)
13. J.I.L. Chen, G. von Freymann, S.Y. Choi, V. Kitaev, G.A. Ozin, J. Mater. Chem. **18**, 369 (2008)
14. J.I.L. Chen, G. von Freymann, S.Y. Choi, V. Kitaev, G.A. Ozin, Adv. Mater. **18**, 1915 (2006)
15. A. Mihi, H. Miguez, J. Phys. Chem. B **109**, 15968 (2005)